

Examining the seismic stress evolution in the face slab of concrete-faced rock-fill dams using dynamic centrifuge tests

Xuedong Zhang, Zitao Zhang*, Yingqi Wei, Jianhui Liang, Jing Hu

State Key Laboratory of Simulation and Regulation of Water Cycle in River Basin, China Institute of Water Resources and Hydropower Research, Beijing, 1000038, China



ARTICLE INFO

Keywords:

CFRD
Dynamic centrifuge tests
Stress in the slab
Extremely strong earthquake
Failure mode

ABSTRACT

This paper aims to characterize the seismic behavior of concrete-faced rock-fill dams. A series of dynamic centrifuge tests were carried out. The experimental results demonstrate that the stress evolution in the face slab is related to the pattern of energy buildup and that the overall stress evolution pattern is highly affected by pre-shaking. For the dams which have not experienced a relatively strong earthquake, compressive and tensile stress increments due to shaking are developed on the outer and inner faces, respectively. However, for the dams which have experienced a relatively strong earthquake, the inner face exhibits an overall tensile stress increment with time while the stress on the outer face only fluctuates around zero with minor overall variation. As for the failure mode under an extremely strong earthquake, slight surface sliding initially occurs, and then rock-fill particles move towards downstream direction, leading to deep sliding and significant dam deformation.

1. Introduction

The concrete-faced rock-fill dam (CFRD) has been widely used all over the world thanks to its advantages including complete usage of local embankment materials, simple detailing and construction, short construction period and cost-effectiveness [1–5]. Recent CFRDs include 196 m-high Karahnjukar Dam in Iceland, 202 m-high Campos Novos Dam in Brazil and 209 m-high La Yesca in Mexico, etc. About 300 CFRDs, nearly accounting for 50% of those dams globally, have been built in China. Among those CFRDs, there are more than 80 dams with a height larger than 100 m including the 233 m-high Shuibuya Dam [4,6,7]. Considering the large dam height, the high amount of reservoir water and large population in the downstream area, it is extremely important to guarantee the safety of CFRDs in China.

Due to the spatial distribution characteristics of hydraulic resources, many CFRDs have been built in high seismic intensity area in China and an increasing number of CFRDs are planned to be built in such area. For example, the design peak ground acceleration (PGA) is 0.394 g for the 247 m-high Dashixia dam which is under construction in Xinjiang Province, while the PGA of the maximum credible earthquake (MCE) level is as high as 0.477 g. It is usually believed that the CFRDs are inherently more resistant to earthquake loading compared with earth-core rock-fill dams due to the fact that severe pore-water pressure build-up and soil strength reduction can hardly occur during earthquake

shaking [2,4,5]. However, the 156 m-high Zipingpu dam has been obviously damaged during 2008 Sichuan earthquake measuring 8.0 on the surface wave magnitude M_s scale. The damages include about 1 m crest subsidence, severe horizontal displacement at crest as large as 20 cm, cracking between downstream slope and dam crest road pavement, crushed damage to the face joints, distortion of steel bars of construction joints in the face slab, etc [8–10]. This aroused public concerns and the attention of geotechnical engineers and scholars to the seismic behavior of CFRDs. Hence, there is an increasing need in engineering practice to obtain a better understanding of the seismic performance of CFRDs in order to improve the seismic design of those dams.

Many insights into the seismic behavior of CFRDs have been obtained using shaking table tests on small-scale models [11–13]. However, as pointed out by Uddin et al. [14], the results from those tests should be viewed with great caution, and only qualitatively due to the fact that the effects of gravity on material behavior cannot be taken into account. In addition, various numerical methods have been adopted in simulating the seismic behavior of CFRDs [5,14–19]. Numerical simulation is proven to be a powerful tool to provide useful insight into the seismic behavior of CFRDs. However, this relies on the condition that all the aspects in the simulations in terms of the simulation configuration, the boundary conditions, the constitutive models and the associated parameters are accurately determined. In addition, dynamic centrifuge tests are used to study such a problem. Unlike shaking table

* Corresponding author.

E-mail addresses: ytxd@iwhr.com (X. Zhang), zhangzt@iwhr.com (Z. Zhang), weiyq@iwhr.com (Y. Wei), liangjh@iwhr.com (J. Liang), hujing@iwhr.com (J. Hu).

Table 1
Summary of previous dynamic centrifuge tests on CFRDs published in the literature.

| Case No. | Centrifugal acceleration (g) | Model dam height H_{m0} (mm) | Reservoir water height/ H_{m0} (mm) | Concrete face slab model | Waveform of the input motion | Prototype duration of the input motion (s) | Prototype peak bedrock acceleration PGA (g) | Reference |
|----------|------------------------------|--------------------------------|---------------------------------------|---------------------------------|------------------------------|--|---|----------------------------|
| 1 | 50 | 111 | 0, ~0.9 | Aluminum sheet | Sinusoidal wave | 10 | 0.3 | Wang & Zhang (2003) |
| 2 | 40 | 160 | 0.9 | High-density polyethylene sheet | Ofunato earthquake wave | 14 | 0.1–0.57, 8 stages | Kim et al. (2011) |
| 3 | 50 | 180 | 0, 0.94 | Aluminum sheet | Parkfield earthquake wave | 50 | 0.034, 0.13 | Cheng & Zhang (2011, 2012) |

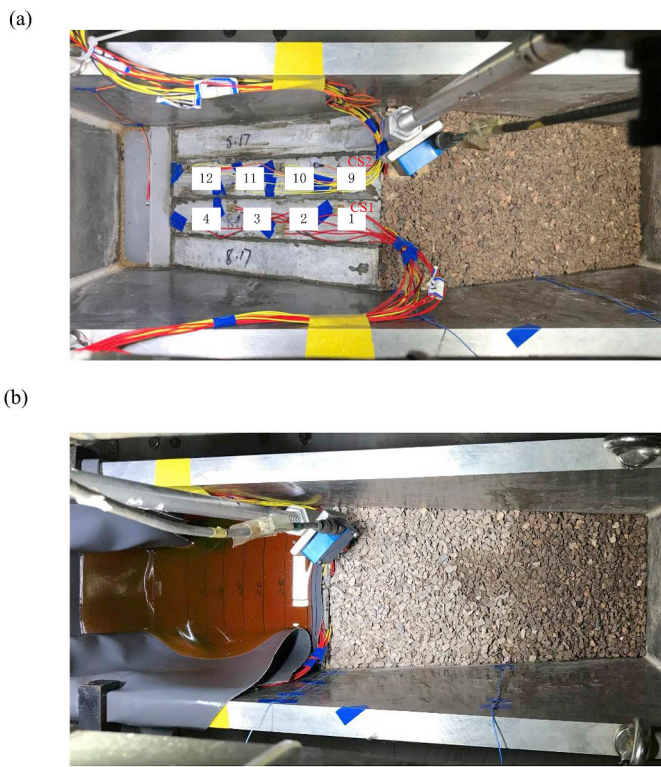


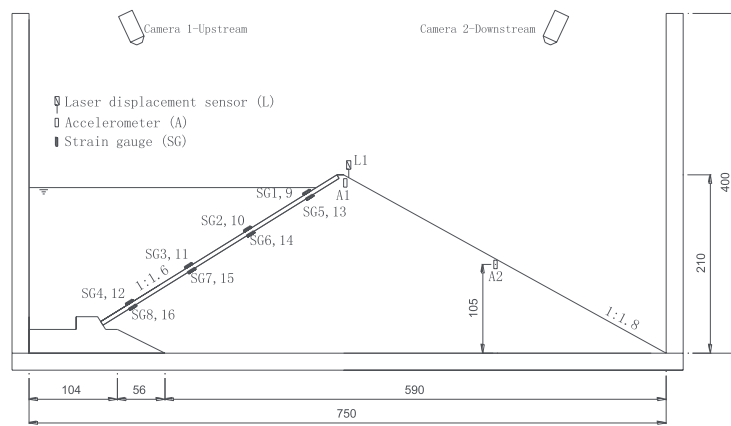
Fig. 1. Pictures of (a) the CFRD model with empty reservoir in Group 1 and (b) the model with high reservoir water level in Group 2.

tests, the prototype stress field can be reproduced in dynamic centrifuge tests, hence, the effects of gravity on material behavior can be taken into account, and the physical properties of the geotechnical material in dynamic centrifuge tests resemble the prototype properties. Therefore, dynamic centrifuge modelling is believed to be an efficient and advantageous tool for investigating the seismic behavior of CFRDs [14,20]. Meanwhile, the unique observations during dynamic centrifuge tests can be used to validate the constitutive models, procedures and results of numerical modelling.

Table 1 summarizes previous dynamic centrifuge tests on CFRDs published in the literature. Many insights into the acceleration response, dam deformation and the strain and stress evolution in the face slab induced by earthquakes have been obtained in those tests. However, some experimental results associated with the strain and stress evolution in the face slab seem controversial. For example, Wang & Zhang [21] demonstrated that the compressive strain increment is limited but the tensile strain increment can reach 7% on the inner face of the slab during shaking. However, Cheng & Zhang [20,22] and Kim et al. [23] proved that both compressive and tensile stress increments were developed in the face slab due to shaking. In addition, the effect of pre-shaking on the stress evolution in the face slab during shaking need to be further investigated. Therefore, more systematic dynamic centrifuge tests are needed to re-characterize the stress evolution in the face slab during shaking. In addition, only limited dam deformation and surface sliding are observed in previous tests. The failure mode of CFRDs subjected to an extremely strong earthquake still needs to be explored.

This paper aims to characterize the seismic behavior of CFRDs in terms of the stress evolution in the face slab during shaking and the failure mode of CFRDs under an extremely strong earthquake. A series of dynamic centrifuge tests were performed using IWHR (China institute of water resources and hydropower research) centrifuge shaker. The experimental details including model configuration, instrumentation layout and shaking events are firstly presented, followed by results and discussions. At last, a summary on the stress evolution in the face slab is given and some conclusions are drawn.

(a)



(b)

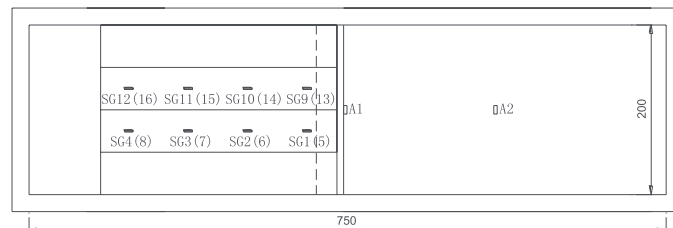


Fig. 2. Schematic drawings of the (a) elevation and (b) plan views of the layout of the centrifuge model and instruments in Group 2. A similar layout is used in Group 1 except that the reservoir remains empty during shaking.

2. Experimental details

The dynamic centrifuge tests were carried out using the IWHR beam centrifuge equipped with a centrifuge shaker. The centrifuge has a capacity of 450 g-ton, a radius of 5.03 m, a maximum centrifugal acceleration of 300 g and a maximum payload mass of 1, 500 kg. The centrifuge shaker can operate up to 100 g centrifugal acceleration with a payload mass up to 440 kg [24]. The shaker can simultaneously simulate horizontal and vertical bedrock motions with peak accelerations up to 30 g and 20 g in the model scale, respectively. In this study, only horizontal dynamic excitation was used in all the tests. Based on the scaling laws for dynamic models, the experimental data can be converted to prototype scale. A centrifugal acceleration 40 g where g is the gravitational acceleration is applied in all the tests, i.e., $N = 40$.

2.1. Centrifuge model configuration

Figs. 1 and 2 give the pictures and schematic drawings of the configuration of the centrifuge models. A rectangular rigid container box with inner dimensions of 0.75 m (length) \times 0.2 m (width) \times 0.4 m (height) was used to accommodate the centrifuge models. Using such a rigid box may affect the model characteristics, however, as pointed by Park and Kim [25], the effect is not considered to be significant once appropriate lubrication has been applied between the model and the side walls.

The centrifuge model with an empty reservoir was firstly prepared. As shown in Figs. 1a and 2, the configuration of the CFRD model was designed according to a CFRD which is under construction in China. The model is mainly composed of rock-fill zone, sand cushion layer,

face slab and toe wall. The upstream and downstream slopes of the dam model were 1:1.6 and 1:1.8, respectively. With a model height (H_{mo}) of 210 mm, the dam model simulates a CFRD with a prototype height (H_0) of 8.4 m at a centrifugal acceleration of 40 g. The prototype height is relatively small compared with that generally used in the field. This is mainly restricted by the limited size of container, centrifugal acceleration capacity and payload mass capacity of the centrifuge shaker. Nevertheless, the prototype height is close to those used in previous centrifuges tests by Refs. [20–23]. The experimental results are believed reliable to reflect the seismic behavior of CFRDs.

As for the procedures in the model preparation, a custom-made toe wall using PVC (Polyvinyl chloride) material with a density of 1.6 g/cm³ and a Young's modulus of about 2 GPa was firstly placed on the bottom of the container. The toe wall is used herein to ensure that the face slab is supported in a way similar to that used in the field. After the placement of the toe wall, the rock-fill zone was constructed using the rock-fills collected from a dam construction site in China. Due to restriction of the width of the container, particles larger than 10 mm were removed by sieving. The model rock-fill material is composed of 77% of particles with sizes of 5–10 mm and 23% of those finer than 5 mm. The mass fraction of particles finer than 5 mm is the same as that used in the site. According to Seed et al. [26], the shear modulus at the same strain level decreases with decreasing particle sizes at the same confining pressure and void ratio. Hence, the model rock-fill material seems softer than the prototype material, and the seismic deformation of the prototype dam might be over-estimated based on the centrifuge results. In order to minimize the slippage between the bedrock and the dam body, a layer of rock-fill particles was firstly glued onto the base plate. The side walls were covered with petrolatum in order to minimize the

Table 2
Summary of the dynamic centrifuge tests carried out in this study.

| Group | Reservoir water condition | Test No. | Centrifugal acceleration (g) | Dam model height H_{mo} (mm) | Reservoir water height/ H_{mo} (mm) | Concrete face slab model | Prototype input ground motion characteristics | | | |
|------------------|---------------------------|------------------|------------------------------|--------------------------------|---------------------------------------|--------------------------|--|---------|-------------------------------------|-----------------------------|
| | | | | | | | Waveform | PGA (g) | Significant duration D_{5-95} (s) | Arias Intensity I_a (m/s) |
| Group 1 (spin 1) | Empty reservoir | G1-T1-0.23g | 40 | 210 | 0 | Cement sheet | Synthetic earthquake wave compatible with seismic design spectrum recommended by Chinese code (NB 35047-2015), Fig. 3a | 0.23 | 16.6 | 1.3 |
| | | G1-T2-0.26g | | | | | | 0.26 | 16.6 | 1.7 |
| | | G1-T3-0.36g | | | | | | 0.36 | 16.1 | 3.4 |
| | | G1-T4-0.24g-R1 | | | | | | 0.24 | 16.1 | 1.5 |
| | | G1-T5-0.33g-R2 | | | | | | 0.33 | 16.3 | 3.0 |
| | | G2-T1-0.46g | | | | | | 0.46 | 49.4 | 13.8 |
| | | G2-T2-0.59g-SINE | | | | | | 0.59 | 59.3 | 90.3 |
| | | | | | | | | | | |

friction between the dam model and the side walls of the container, and then the rock-fill material was placed and compacted layer by layer until the dry density reached $1,990 \text{ kg/m}^3$, which is close to the value used in practice. In order to improve the efficiency of compaction, the dry rock-fill material is mixed with water, and the water content is about 7%. When the thickness of the whole rock-fill layer reached 210 mm, a careful excavation was carried out to produce the geometry of the rock-fill zone as shown in Fig. 2. Afterwards, a cushion layer with a thickness of 5 mm was prepared along the upstream slope using fine sand, followed by the installation of the face slab consisted of 4 cement sheets. Each cuboidal sheet has a length of 33 cm, a width of 5 cm, a thickness of 5 mm and a height of 17.3 cm in model scale. The prototype height of the face slab is 6.9 m at a centrifugal acceleration of 40 g. The density, elastic modulus and compressive strength measured at the same day as the dynamic centrifuge tests were $2,400 \text{ kg/m}^3$, 27.3 GPa and 43.8 MPa, respectively. Those values were close to the general values used at practice in China.

The centrifuge model with empty reservoir was subjected to a series of shaking events in Group 1 at a centrifugal acceleration of 40 g. Minor deformation was induced by the shaking events and by spin-up and spin-down of the centrifuge. Hence, after completing those shaking events in Group 1 and spin-down of the centrifuge, the rock-fills at shallower locations of the downstream slope were firstly loosened and then re-compacted in order to erase the pre-shaking effect, and then the same model was used to prepare the centrifuge model with high reservoir water level in Group 2. Considering that the rock-fill zone of a CFRD is generally dry and the seepage flow inside the dam body is limited in the field, no seepage flow through the spacing between adjacent cement sheets and through the boundaries between the face slab and the box should be allowed. However, it is extremely difficult to make the spacing impermeable during spin-up of centrifuge as well as during the subsequent shaking events in Group 2. Hence, following the procedure used in Refs. [20–23], a thin membrane was placed on the upstream slope to obstruct seepage, and then the reservoir was filled with water to 93% of the dam height to simulate the condition with high reservoir water level. Due to the limitation from the box size, the dimension of the reservoir water in the longitudinal direction is relatively small compared with the case in the field, which may lead to higher water pressure on the dam and stronger water swell during shaking.

2.2. Instrumentation layout

All the centrifuge models were instrumented in a similar way using accelerometers, laser displacement sensors and strain gauges. Two accelerometers (Model 352A24, PCB Piezotronics, Inc., USA) denoted as A1 and A2 were installed along the downstream slope at heights of $0.95H_{mo}$ and $0.5H_{mo}$ to monitor the horizontal accelerations. In order to measure the settlement at crest, a laser displacement sensor denoted as L1 was installed near dam crest. Moreover, as shown in Figs. 1a and 2, the outer and inner faces of the cement sheet CS1 were instrumented with the strain gauges SG1 to SG4 and those from SG5 to SG8, respectively. The four pairs of strains, i.e., SG1 & 5, SG2 & 6, SG3 & 7 and SG4 & 8, were used to obtain the strains and stresses in the face slab at four heights of $0.90H_{mo}$, $0.69H_{mo}$, $0.49H_{mo}$ and $0.28H_{mo}$. The other cement sheet CS2 as shown in Fig. 1a was instrumented with the strain gauges from SG9 to SG16 in a similar way.

2.3. Shaking events

As previously mentioned, the centrifuge models were subjected to a series of horizontal bedrock motions or shaking events perpendicular to the dam axis along the longitudinal direction of the container at a centrifugal acceleration of 40 g. Table 2 summarizes the dynamic centrifuge tests carried out in this study. The waveform used in Group 1 was a synthetic acceleration time history compatible with seismic

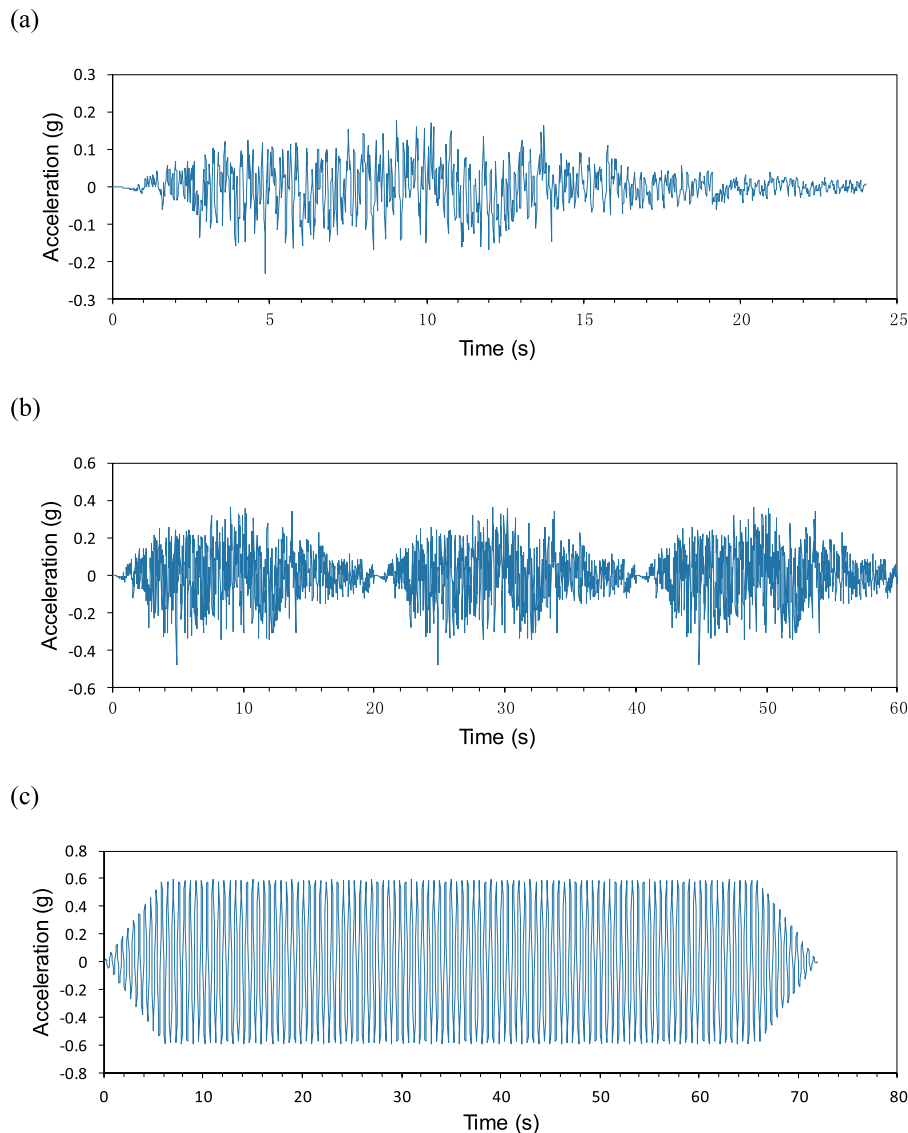


Fig. 3. The waveforms of the input motion in prototype scale: (a) a synthetic earthquake wave compatible with seismic design spectrum by Chinese code used in Group 1; (b) a synthetic earthquake wave with three successive shocks used in G2-T1-0.46 g; (c) a screened sinusoidal wave used in G2-T2-0.59 g-SINE.

design spectrum recommended by Chinese code [27] as shown in Fig. 3a. As shown in Table 2, the shaking events in Group 1 were denoted by G1-T1-0.23 g, G1-T2-0.26 g, G1-T3-0.36 g, G1-T4-0.24 g-R1 and G1-T5-0.33 g-R2, where the number following “T” indicates the excitation sequence number and the number before “g” represents the prototype PGA of the input motion measured by the accelerometer on the centrifuge shaking table. Only the amplitudes have been changed in the motions in Group 1. PGA increased from 0.23 g to 0.36 g in the initial three tests, and then smaller PGAs 0.24 g and 0.33 g were used in the last two tests. Comparison between the experimental results from the initial three tests and the last two tests are used to examine the effect of pre-shaking by the relatively strong earthquake in G1-T3-0.36 g. The experimental results can enhance the understanding on the seismic behavior of dams subjected to aftershocks following the main shock in real earthquake events. In Group 2, the model was firstly subjected to a synthetic earthquake wave with three successive shocks as shown in Fig. 3b, and the measured PGA was 0.46 g. The waveform of each shock was the same as that observed in the initial 20 s in each test in Group 1, and the duration 20 s was slightly smaller than that used in Group 1, i.e., 24 s. After that, a screened sinusoidal wave as shown in Fig. 3c was used, and the measured PGA was as high as 0.59 g,

making it possible to examine the seismic behavior under an extremely strong earthquake. The two tests were denoted as G2-T1-0.46 g and G2-T2-0.59 g-SINE.

The experimental results from both groups are presented and discussed separately in the following. All the results are presented in prototype units unless indicated otherwise.

3. Results and discussions: group 1

The input ground motions measured by the accelerometers on the shaking table are firstly compared to verify the similarity of the waveforms in all the shaking events, and then the seismic behavior is discussed with a particular focus on the stress evolution in the face slab during shaking.

3.1. Comparison of input ground motions

Fig. 4 presents the bedrock acceleration $a(t)$ measured by the sensor on the shaking table during each shaking event in Group 1. The similarity of those waveforms can be verified by the temporal evolution of Arias Intensity, which is an index representing the energy of the ground motion and given by

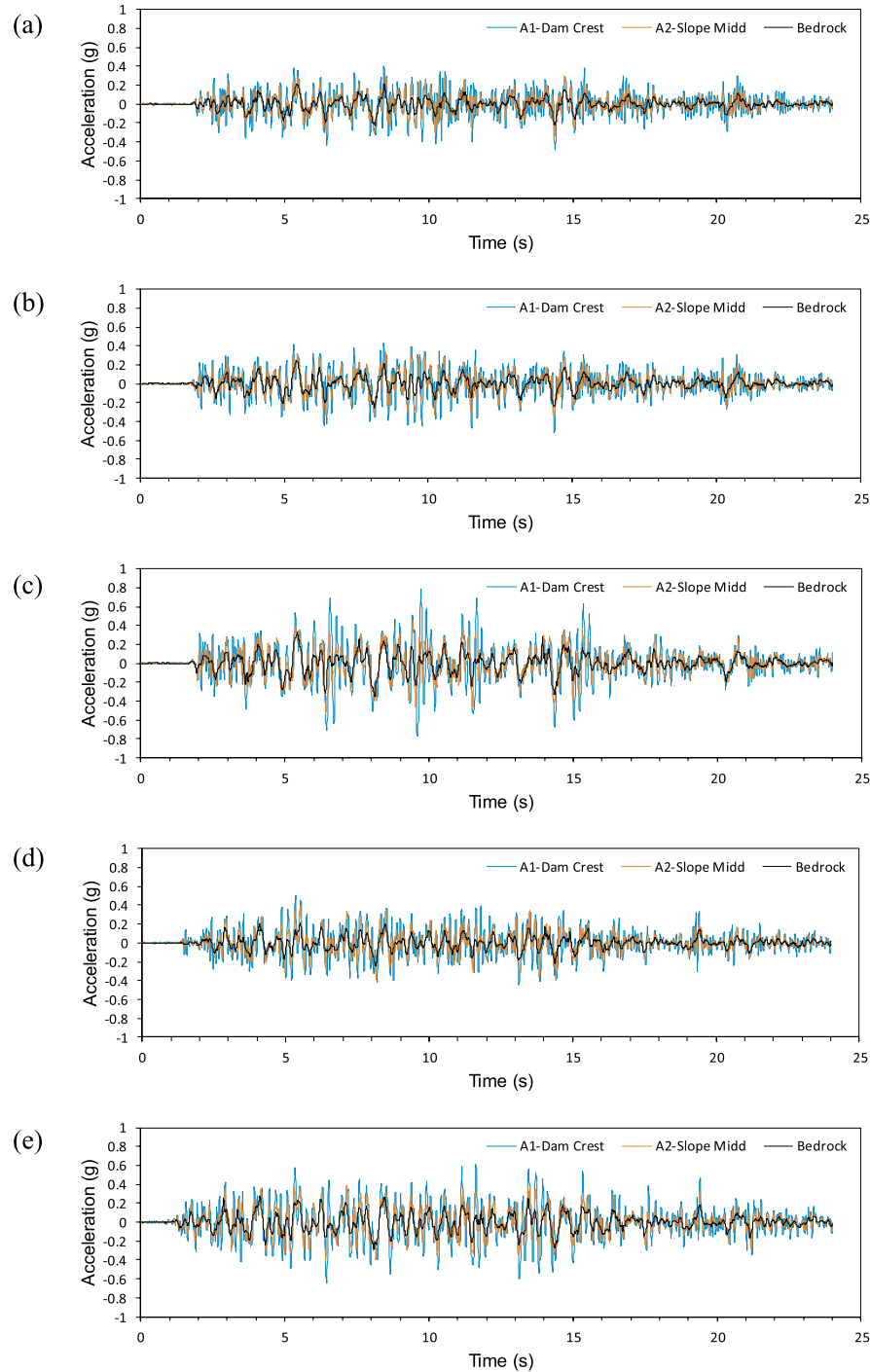


Fig. 4. Acceleration records on the shaking table and at different heights along the downstream slope during (a) G1-T1-0.23 g, (b) G1-T2-0.26 g, (c) G1-T3-0.36 g, (d) G1-T4-0.24 g-R1 and (e) G1-T5-0.33 g-R2.

$$I_a(T) = \frac{\pi}{2g} \int_0^T a^2(t) dt \quad (1)$$

over the time period from 0 to T . Fig. 5a presents the variation in Arias Intensity during each shaking. The final value of Arias Intensity at the end of each shaking increases from 1.3 to 3.4 m/s as PGA increases from 0.23 g to 0.36 g in the initial three tests. In the last two tests, the value increases from 1.5 to 3.0 m/s as PGA increases from 0.24 g to 0.33 g. Fig. 5b presents the normalized Arias Intensity with respect to its final value. Reasonable agreement between the normalized I_a – time histories proves the similarity in the waveforms of the input ground motions. The significant duration $D_{5.95}$, i.e., the time duration for the change in

normalized Arias intensity from 5% to 95%, is further obtained. As expected, the values of $D_{5.95}$ are in a narrow range from 16.1 to 16.6 s in those tests.

3.2. Acceleration amplification and crest settlement

As shown in Fig. 4, the acceleration increases with height in the rock-fills, and the acceleration amplification factor at crest and that at the middle of the slope are in the ranges of 2.02–2.31 and 1.40–1.62, respectively. This reflects the acceleration amplification behavior similar to that observed in Refs. [20,22]. The acceleration amplification

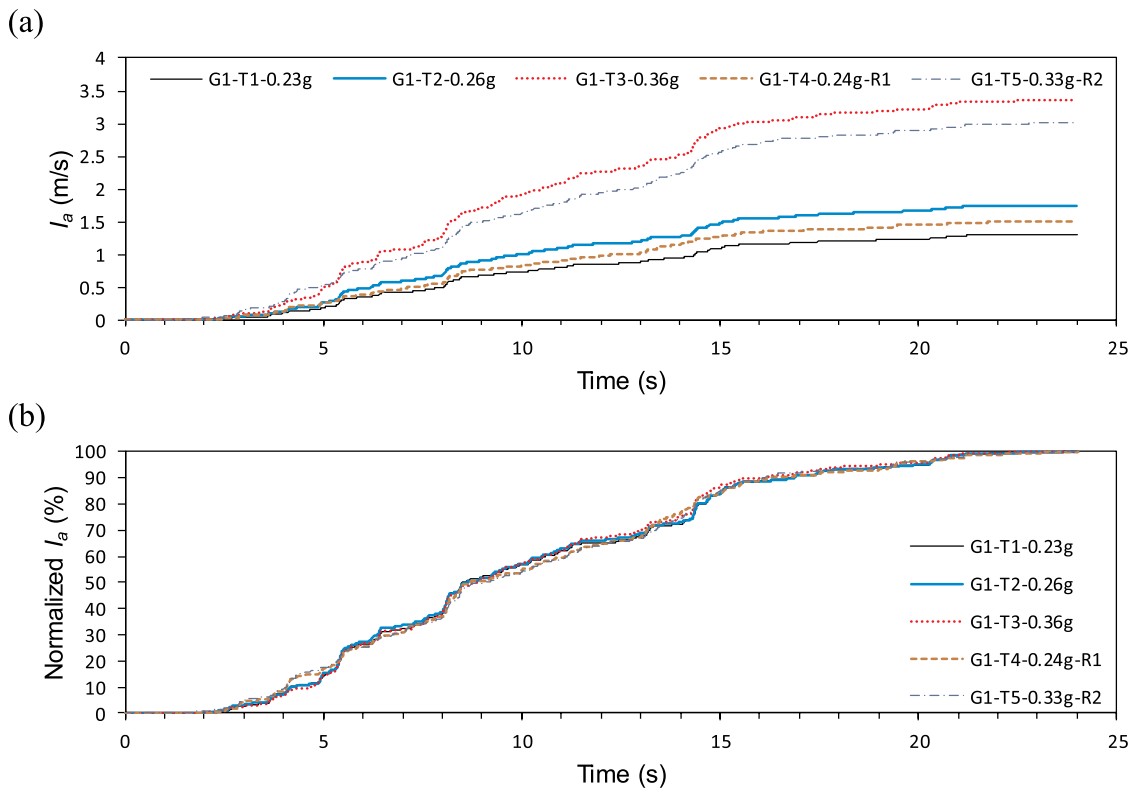


Fig. 5. Histories of (a) Arias intensity I_a and (b) normalized I_a during the shaking events in Group 1.

factor increases with increasing PGA at crest, which is also consistent with the experimental results in Ref. [23]. As for the crest settlement measured by the laser displacement sensor, the maximum crest settlement due to shaking is observed in G1-T3-0.36 g, and the value equals 0.14% of dam height. Such small settlement behavior is consistent with the observation in Ref. [23] where small crest settlements (< 0.21% of dam height) for bedrock acceleration up to 0.2–0.35 g is observed. As for damages on the rock-fill slope, the recorded pictures indicate that only slight surface sliding occurs near dam crest at a bedrock acceleration of 0.36 g while minor surface sliding occurs at smaller bedrock acceleration.

3.3. Stress evolution in the face slab in the initial three tests

The net change in stress $\Delta\sigma$ due to shaking is selected to represent the stress evolution in the face slab. That is, the initial stress before the specific shaking is subtracted in the value of $\Delta\sigma$. A positive value of $\Delta\sigma$ indicates that the material of the face slab is further compressed which leads to the development of compressive stress increment at the monitoring point, while a negative value represents tensile stress increment.

Fig. 6a and b presents $\Delta\sigma$ -time histories on the outer and inner faces of CS1 during G1-T1-0.23 g, respectively. The stress evolution in CS2 are given in Fig. 6c and d. Due to a data acquisition problem, there lacks data from strain gauges SG1, SG8 and SG12. Both compressive and tensile stress increments are developed in the face slab, which is consistent with [20–23]. The overall trend of the stress evolution on the outer face is that compressive stress increment due to shaking increases with time as shown in Fig. 6a and c, while the tensile stress increment is developed on the inner face as shown in Fig. 6b and d. Such overall trend becomes more obvious during a much stronger shaking event in G1-T3-0.36 g as shown in Fig. 7. Since the overall trend during G1-T2-0.26 g is similar to those shown in Figs. 6 and 7, the associated results from G1-T2-0.26 g is not presented due to space limitations. Such kind of stress evolution suggests that crushing of the face slab may emerge on the outer face, while tensile cracking may start from the inner face.

Another feature of the stress evolution is that the change in $\Delta\sigma$ mainly occurs from 3 to 14 s. This is related to the pattern of energy buildup in terms of the evolution of the energy buildup rate during each shaking event. The rate of energy buildup can be roughly represented by the slope of $\Delta I_a/\Delta T$ [28]. As shown in Fig. 5a, I_a initially increases with time in an extremely low rate, and then the rate becomes much larger from 3 to 14 s. Afterwards, the rate becomes relatively small until the end of each shaking event. Therefore, most of the change in $\Delta\sigma$ occurs from 3 to 14 s due to the high rate of energy buildup.

In order to examine the spatial distribution of the stress increment along the face slab, the peak values ($\Delta\sigma_{peak}$) of the compressive and tensile stress increments are determined. As shown in Fig. 8, both compressive and tensile values of $\Delta\sigma_{peak}$ increase with increasing height in all the three tests. As the rock-fills at higher locations experience stronger seismic motions, the rock-fill deformation is relatively large at those locations, leading to relatively large stress increments due to shaking. In addition, the change of tensile $\Delta\sigma_{peak}$ on the inner face with height is larger than that of compressive $\Delta\sigma_{peak}$ on the outer face. Comparison between the tensile and compressive values of $\Delta\sigma_{peak}$ at the same elevation indicates that the tensile $\Delta\sigma_{peak}$ is larger than the compressive value.

Fig. 9 shows the effect of PGA on the peak stress increments in the face slab. For the compressive stress increments on the outer faces as shown in Fig. 9a and c, the values of $\Delta\sigma_{peak}$ at higher locations increase with increasing PGA (e.g., SG2, SG9 and SG10), while those at lower locations nearly remain constant with increasing PGA (e.g., SG3, SG4 and SG11). As for the variations of tensile $\Delta\sigma_{peak}$ with PGA, Fig. 9b and d indicate that the peak tensile stress increments increase with increasing PGA at all locations, and the increasing rate is relatively large at higher locations.

3.4. Stress evolution in the face slab in the last two tests

Figs. 10 and 11 present the stress evolutions on the outer and inner faces during G1-T4-0.24 g-R1 and G1-T5-0.33 g-R2, respectively.

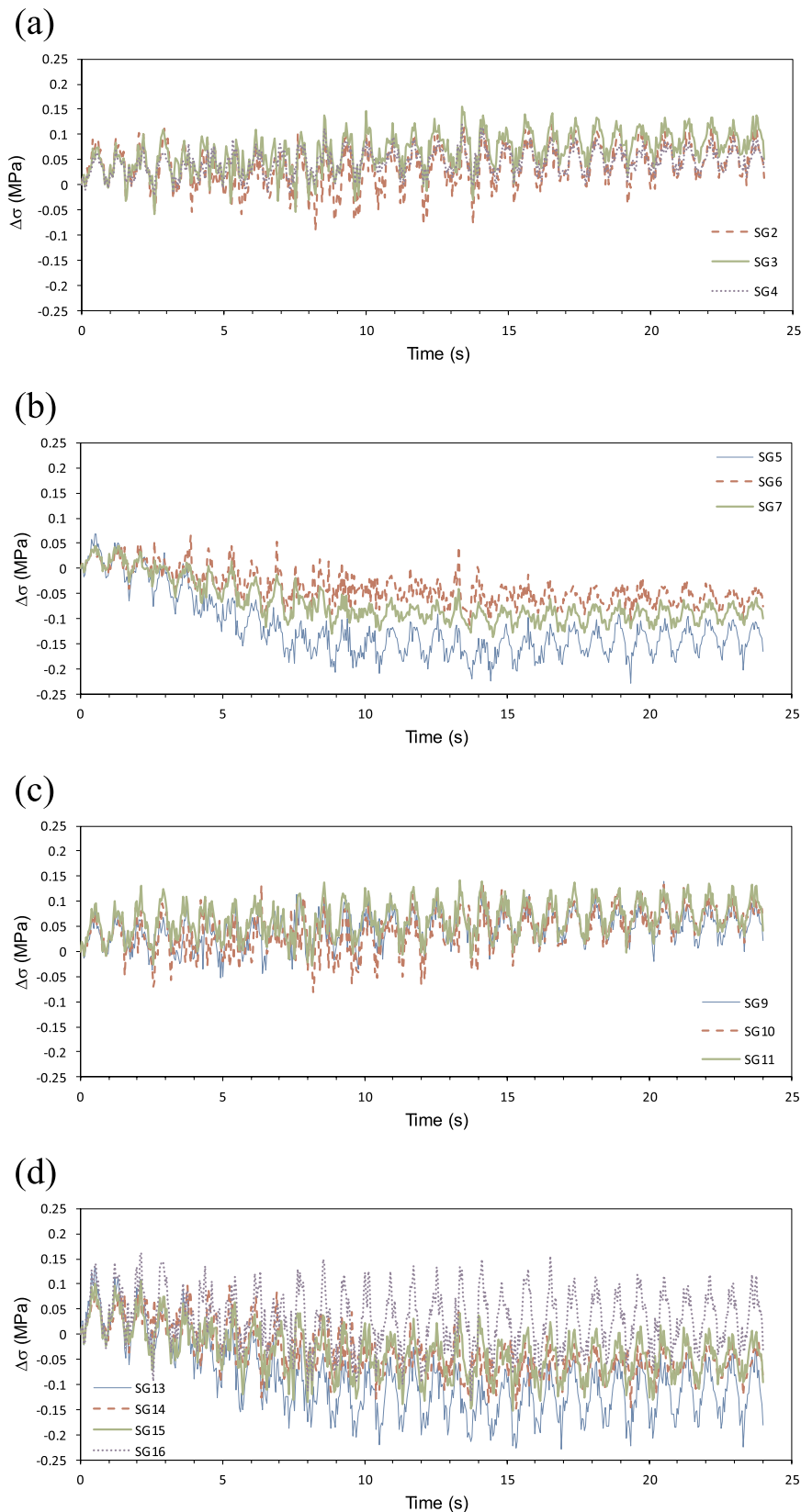


Fig. 6. Stress increments $\Delta\sigma$ due to shaking on the (a) outer and (b) inner faces of CS1 and on the (c) outer and (d) inner faces of CS2 during the dynamic test G1-T1-0.23 g.

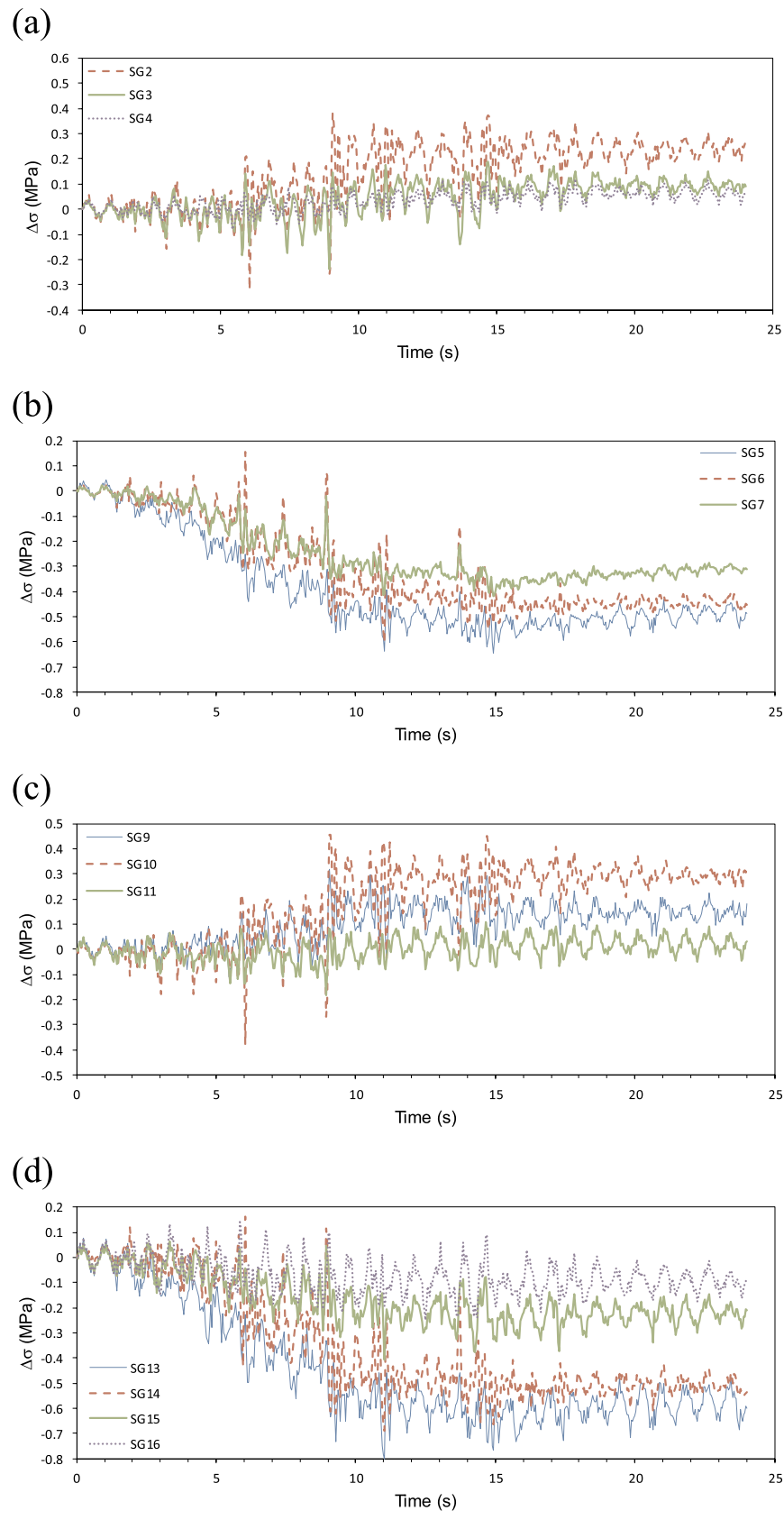


Fig. 7. Stress increments $\Delta\sigma$ due to shaking on the (a) outer and (b) inner faces of CS1 and on the (c) outer and (d) inner faces of CS2 during the dynamic test G1-T3-0.36 g.

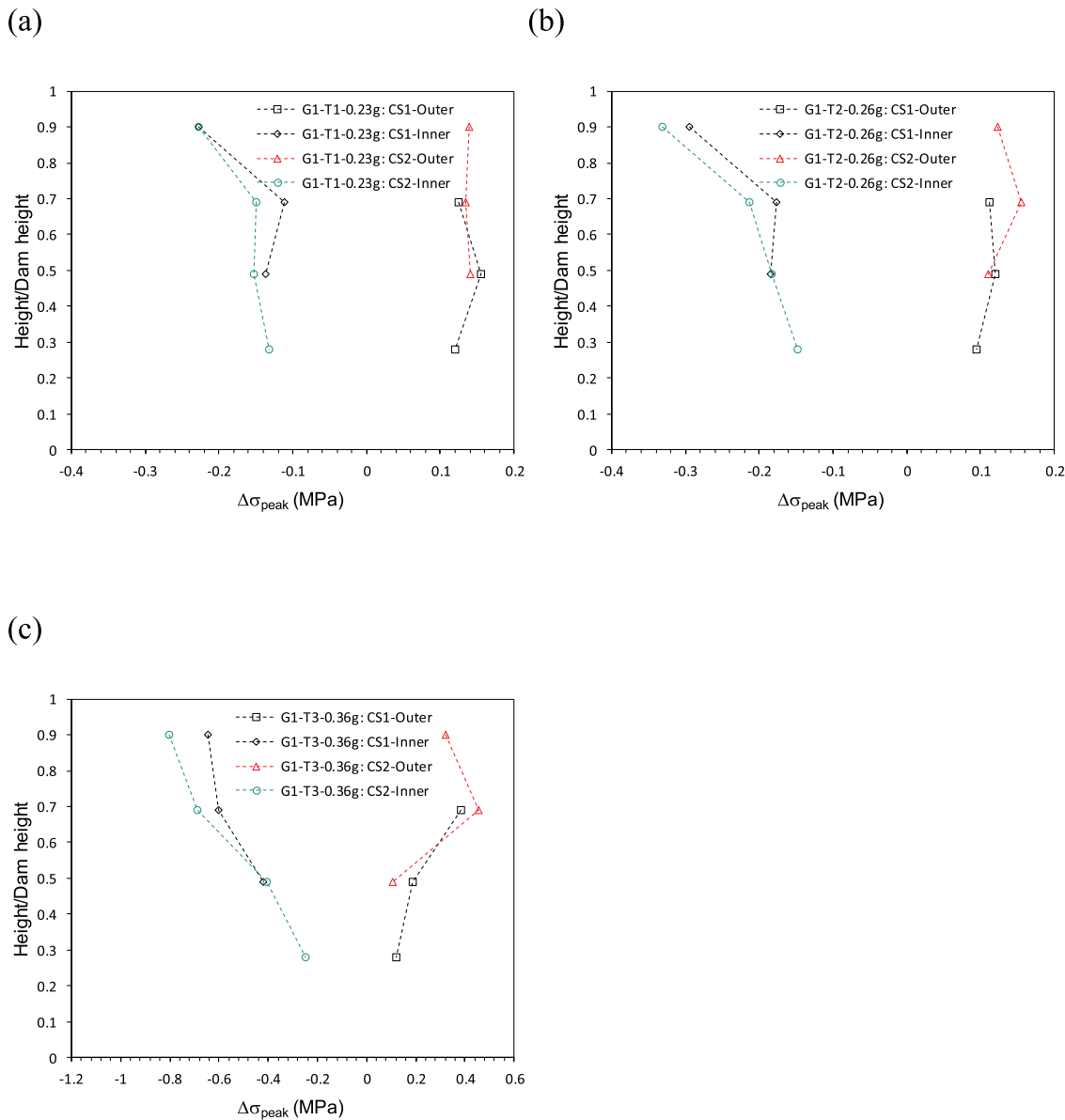


Fig. 8. Distributions of the peak stress increments $\Delta\sigma_{\text{peak}}$ on the outer (compressive) and inner (tensile) faces along the cement sheets: (a) G1-T1-0.23 g; (b) G1-T2-0.26 g and (c) G1-T3-0.36 g.

Similar to the stress evolutions observed in the initial three tests, the inner face exhibits an overall tensile stress increment with time. However, the stresses on the outer face only fluctuate around zero, and the overall change is minor, which is different from those observed in the initial three tests. Hence, less compressive stress increment can be developed on the outer face once the dam has experienced a relatively strong earthquake, leading to smaller risk of crushing damage on the face slab after pre-shaking. Such effect of pre-shaking might be induced by the variation in the dynamic properties of the rock-fills. The magnitude and spatial distribution of the properties of the rock-fills, e.g., shear modulus and damping ratio, may vary after pre-shaking by a relatively strong earthquake, which may result in different rock-fill deformation and stress evolution patterns during shaking.

4. Results and discussions: group 2

As previously mentioned, the centrifuge model was firstly subjected to a synthetic earthquake wave with three successive shocks (Fig. 3b)

and then subjected to a screened sinusoidal wave (Fig. 3c) in Group 2. Fig. 12 presents the evolutions of Arias intensity I_a and normalized I_a of the input ground motions. Based on the histories of normalized I_a , the significant durations of two shaking events are determined as 49.4s and 59.3s, which are much longer than those used in Group 1. The final Arias Intensity at the end of G2-T1-0.46 g is 13.8 m/s, which is four times as large as the maximum value used in Group 1. Although the crest settlement due to shaking $\Delta s/H_0$ is 0.98%, there only occurs surface sliding on the downstream rock-fill slope during shaking. Hence, the experimental results are mainly used to examine the stress evolutions in the face slab. In G2-T2-0.59 g-SINE, the final I_a is as high as 90.3 m/s, which is 6.5 times as large as that used in G2-T1-0.46 g, indicating much more energy of ground motion. Since deep sliding occurs in the downstream rock-fill slope, the experimental results from G2-T2-0.59 g-SINE are mainly used to study the failure mode under an extremely strong earthquake.

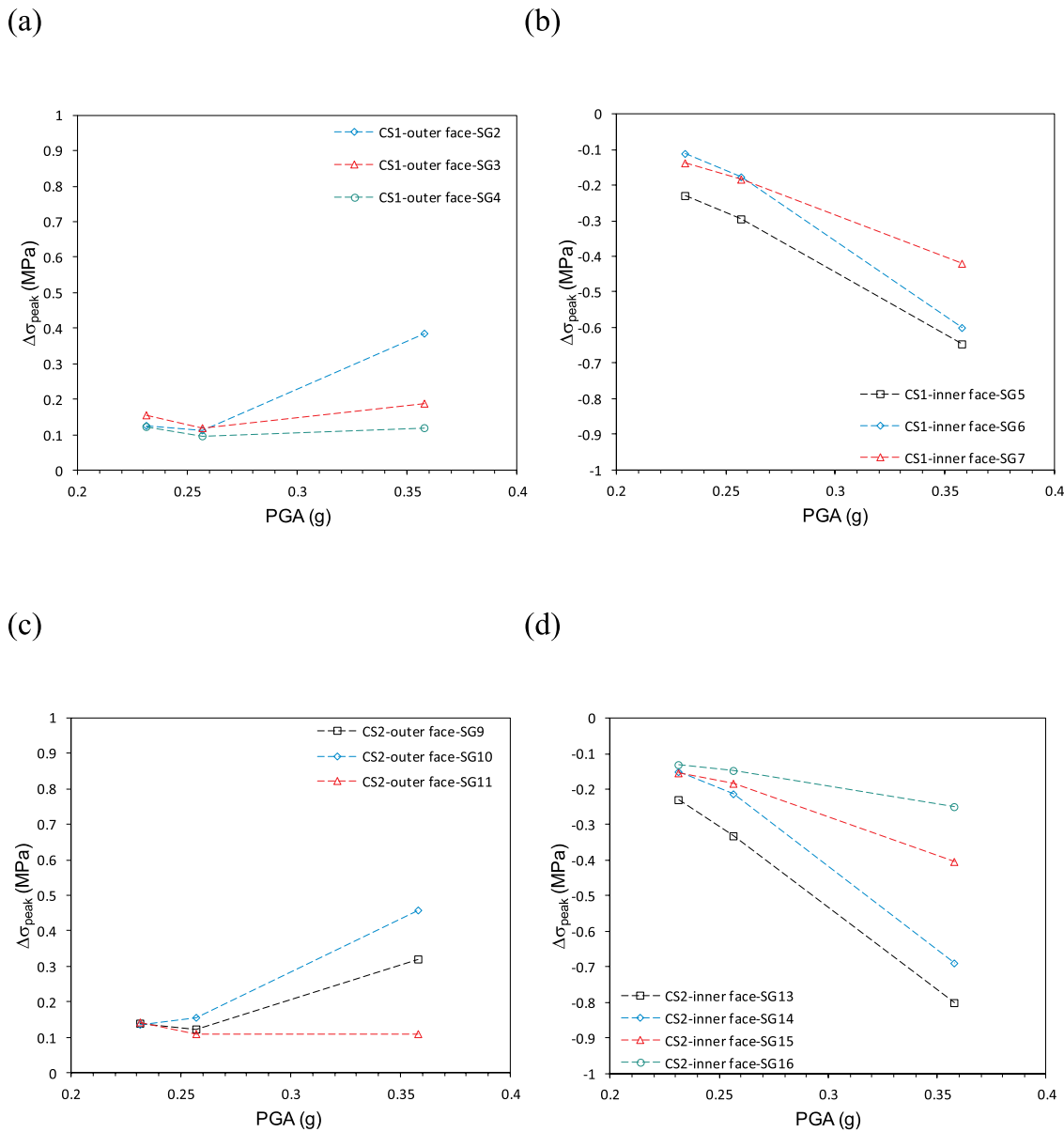


Fig. 9. Variations of peak stress increments $\Delta\sigma_{\text{peak}}$ with PGA for the shaking event in Group 1: (a) compressive value on the outer face of CS1; (b) tensile value on the inner face of CS1; (c) compressive value on the outer face of CS2; and (d) tensile value on the inner face of CS2.

4.1. Stress evolution in the face slab

Fig. 13 presents the stress evolution in the face slab during G2-T1-0.46 g. The overall trend is that the compressive stress increment due to shaking increases with time on the outer face and the tensile stress increment is continuously developed on the inner face. The evolution pattern is similar to that observed in the initial three tests in Group 1. As previously mentioned, the rock-fills at shallower depths of the downstream slope were artificially disturbed after spin-down of the centrifuge following completing the shaking events in Group 1. Such disturbance affects the dynamic properties of rock-fills and eventually erase the effect of pre-shaking on the stress evolution in the face slab.

4.2. Failure mode under an extremely strong earthquake

Fig. 14 presents a picture of the CFRD model and a schematic drawing of its side view after spin-down of the centrifuge following the shaking event G2-T2-0.59 g-SINE. The geometry of the rock-fill zone was manually measured by rulers. The figure shows that the rock-fills

originally located near dam crest have moved towards the downstream direction and then are loosely distributed on the original rock-fill surface. Due to such kind of deep sliding, the rock-fill height is reduced to 85% of its original value after shaking, and the overall slope of the downstream rock-fills becomes much gentler than the original condition.

In order to examine the damage evolution during shaking, the snapshots of the downstream rock-fill slope are collected and presented in Fig. 15. The damage evolution can be divided into three stages. At the first stage from 0 to 3.2 s (Fig. 15a, b and 15c), only slight surface sliding occurs and the dam deformation is limited. The deformation mode is similar to that observed in Group 1 and in G2-T1-0.46 g.

At the second stage from 3.2 to 41.6 s, deep sliding occurs and the rock-fill deformation in this stage contributes to most of the rock-fill deformation due to shaking. The rock-fill particles move in a relatively large velocity in this stage, which can be qualitatively reflected by the snapshots. As shown in Fig. 15c and d, there is an obvious increase in the particle velocity from 3.2 to 4.8 s. The particles move in an even much larger velocity at 12.8 s as shown in Fig. 15e, after which the

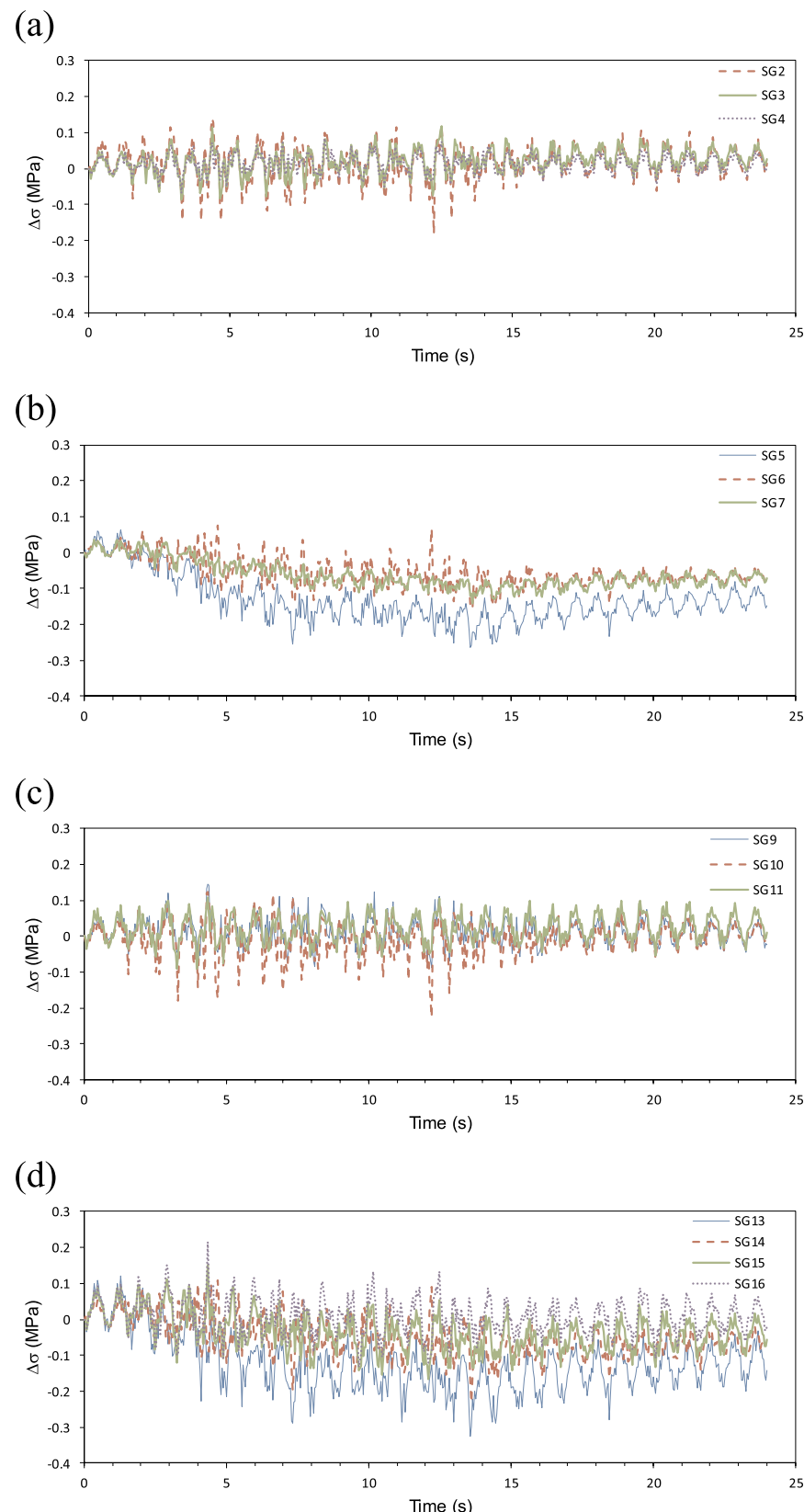


Fig. 10. Stress increments $\Delta\sigma$ due to shaking on the (a) outer and (b) inner faces of CS1 and on the (c) outer and (d) inner faces of CS2 during the dynamic test G1-T4-0.24 g-R1.

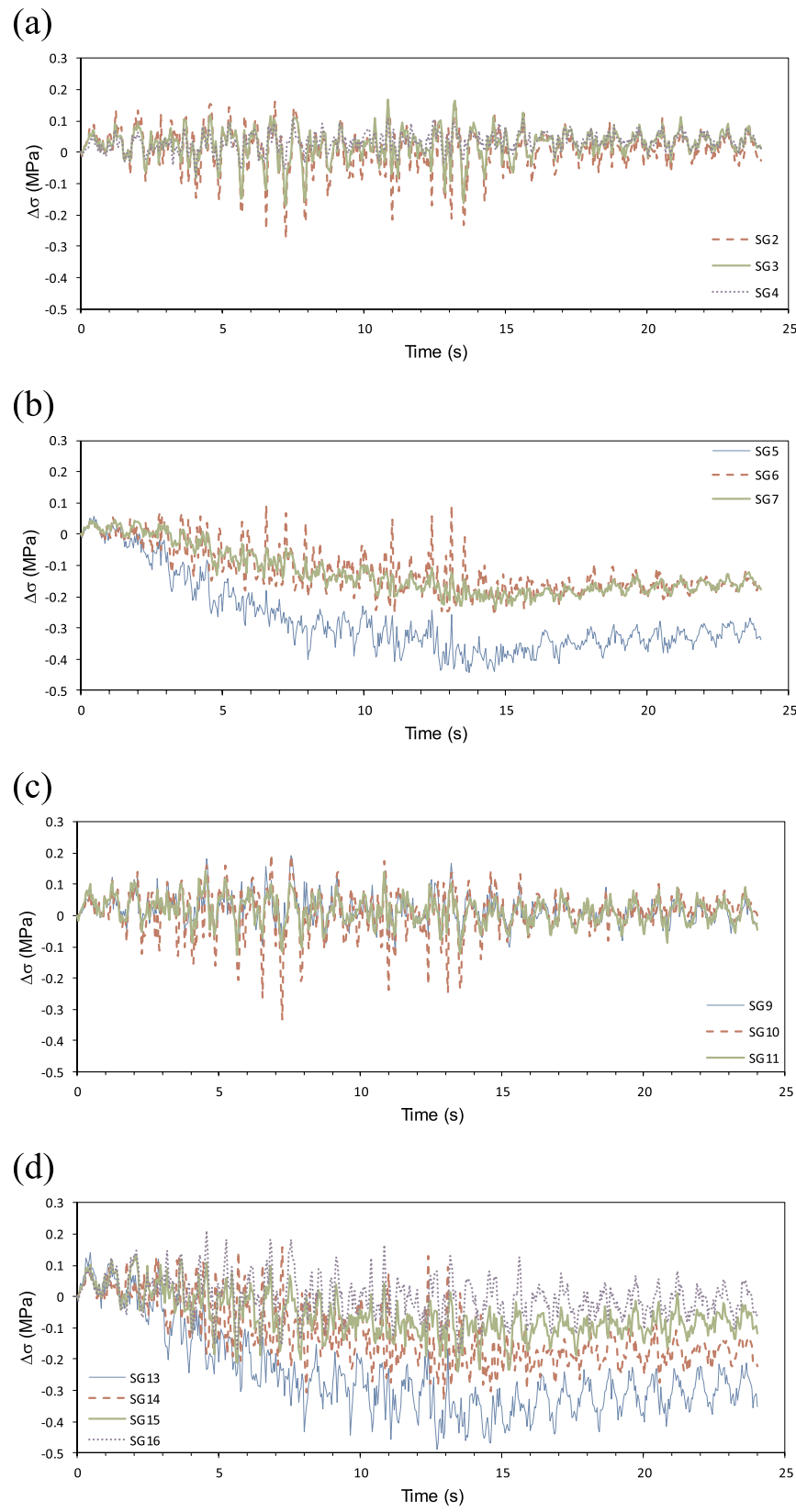


Fig. 11. Stress increments $\Delta\sigma$ due to shaking on the (a) outer and (b) inner faces of CS1 and on the (c) outer and (d) inner faces of CS2 during the dynamic test G1-T5-0.33 g-R2.

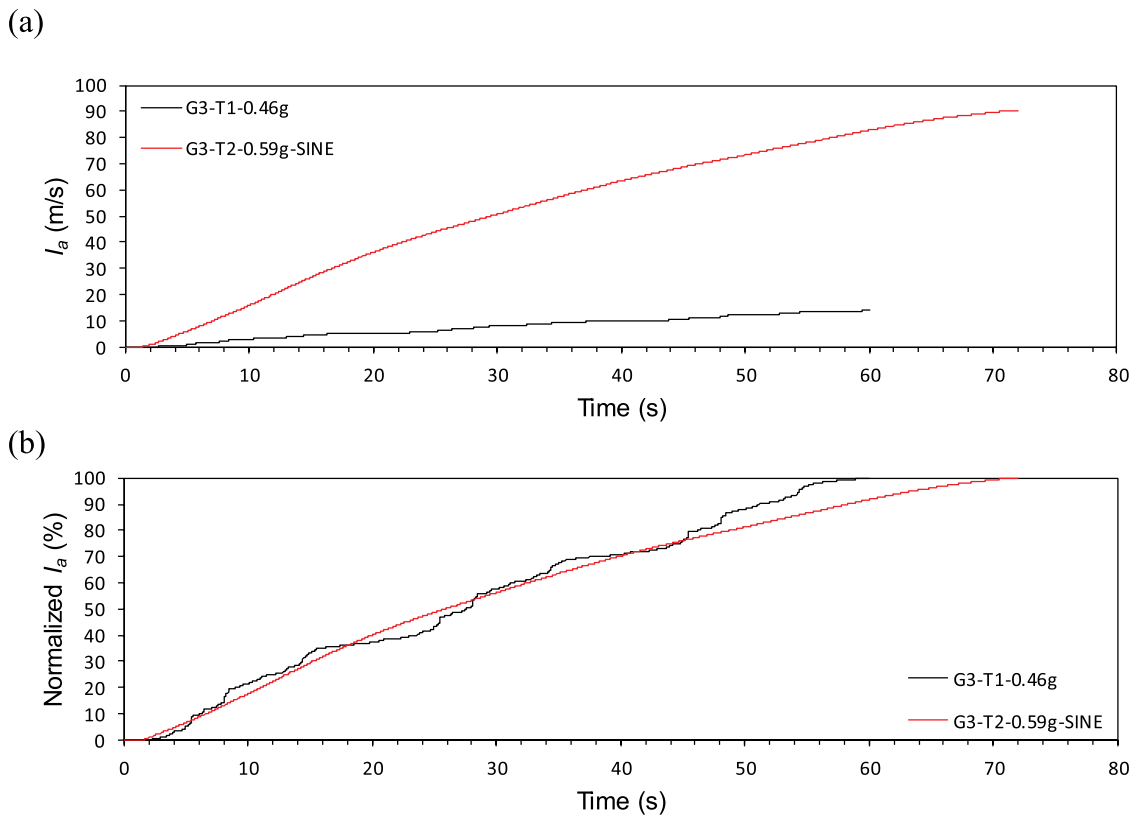


Fig. 12. Histories of (a) Arias intensity I_a and (b) normalized I_a during the shaking events in Group 2.

velocities become smaller (Fig. 15f and g). The movement of particles at dam crest can be shown by the measurements from A1 originally located at dam crest. As shown in Fig. 16a, there is a sudden change in the measurement from A1 at about 3.9 s, after which the measurement is unreliable. The sudden change is induced by the variation in the coupling condition between the sensor and the surrounding rock-fills. This suggests that the sensor and surrounding particles at dam crest start flowing towards downstream direction. Afterwards, the rock-fills at top seem move layer by layer. New rock-fill crest continuously occurs and the rock-fill height keeps decreasing. Due to the movement of rock-fill particles, there lacks support to the sand cushion layer and the face slab. The sands pour towards the downstream direction and cover the new rock-fill crest. However, no damages on the face slab have been observed. As shown in Fig. 17, the overall trend of the stress evolution in the face slab is similar as that observed in G2-T1-0.46 g. Besides the particles near crest, the rock-fills at shallower depths of the downstream slope move towards the downstream direction. As shown in Fig. 16b, there is a sudden change in the measurement from A2 at about 29.5 s, reflecting the significant movement of rock-fill particles at the middle of the downstream slope. The rock-fill particles gradually turn to stable at the end of the second stage. Afterwards, there is minor rock-fill movement and dam deformation at the third stage from 41.6 to 72 s. As for the dam-reservoir interaction, there exists an additional hydrodynamic pressure on the face slab due to the horizontal vibration of the dam under seismic loading. However, such pressure decreases considerably with decreasing slope of the face slab. The numerical simulations in Ref. [15] prove that the hydrodynamic pressure on the face slab can be neglected. Nevertheless, significant water swell has been observed in the test. The increase in the elevation of reservoir water table can be as high as about 15% of the dam height, increasing the risk of overtopping during earthquakes.

5. Summary on stress evolution in the face slab

The experimental results demonstrate two patterns of stress evolution in terms of the overall trend. The first pattern is that compressive and tensile stress increments due to shaking are developed on the outer and inner faces, respectively. This occurs for the CFRDs which have not experienced a relatively strong earthquake. This pattern is observed in the initial three tests in Group 1. As a disturbance on the rock-fills at shallow depths along the downstream slope has been performed before the shaking events in Group 2, the effect of pre-shaking has been fully erased, and the first pattern is also observed in the tests in Group 2. Such kind of stress evolution suggests that crushing of the face slab may emerge on the outer face, while tensile cracking may start from the inner face. The distribution of compressive stress increment on the outer face echoes the crushed damage to the face joints in Zipingpu Dam after Wenchuan earthquake as shown by the results from field investigation in Refs. [8–10]. The second pattern is that the inner face exhibits an overall tensile stress increment with time while the stress on the outer face only fluctuate around zero with minor overall variation. This occurs for the CFRDs which have experienced a relatively strong earthquake. This pattern is observed in the last two tests following G1-T3-0.36 g in Group 1.

6. Conclusions

In this study, a series of dynamic centrifuge tests on CFRDs were carried out in order to examine the temporal evolution of stresses in the face slab and the failure mode or damage evolution under an extremely strong earthquake. Both conditions with an empty reservoir and with high reservoir water level are examined. The input ground motions include a synthetic earthquake wave, a synthetic earthquake wave with three successive shocks and a screened sinusoidal wave. The PGAs of the input motions are in a range of 0.23–0.59 g, and the range of final Arias Intensity is much wider than that in previous tests. The maximum

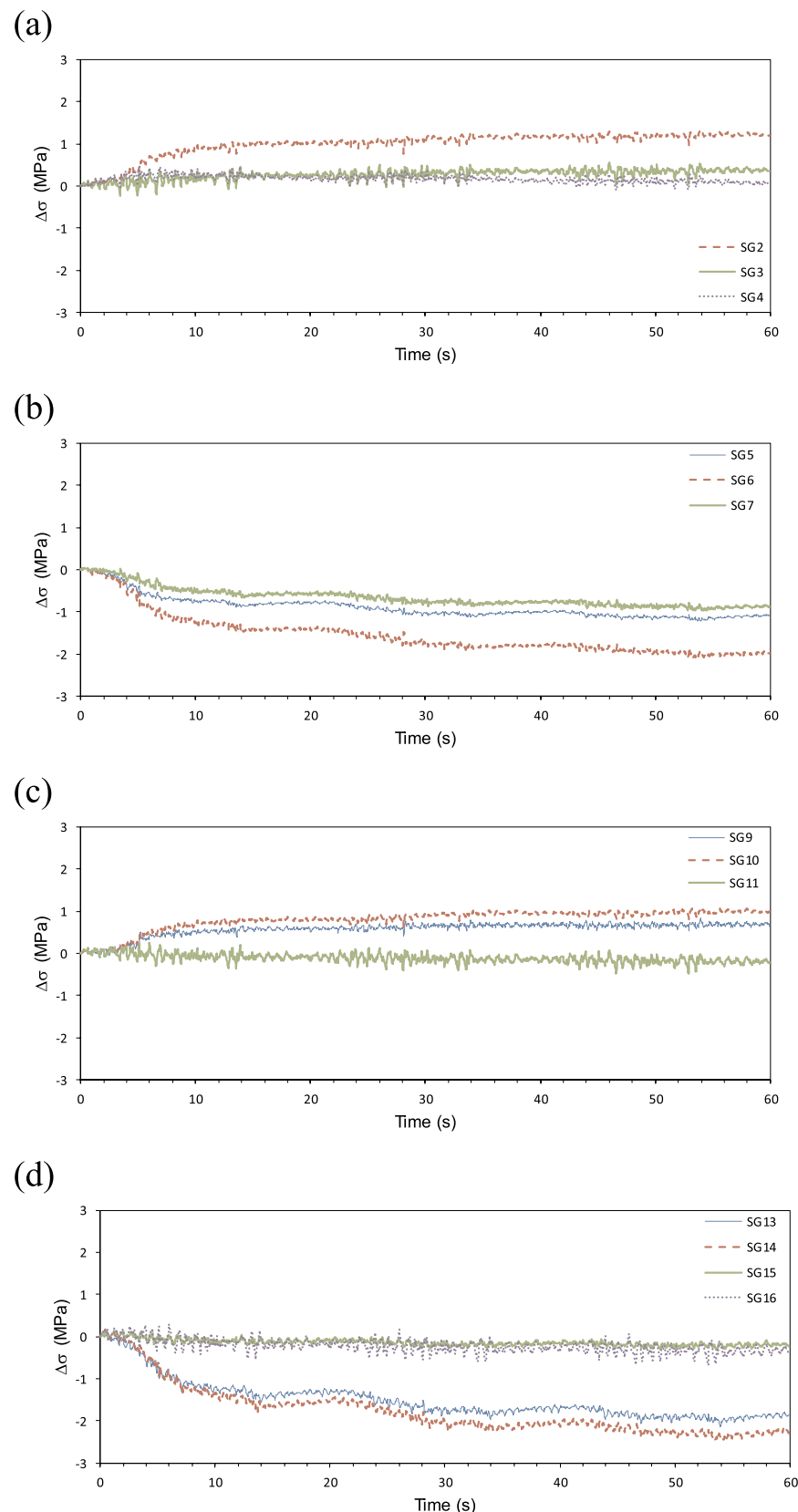


Fig. 13. Stress increments $\Delta\sigma$ due to shaking on the (a) outer and (b) inner faces of CS1 and on the (c) outer and (d) inner faces of CS2 during the dynamic test G2-T1-0.46 g.



Fig. 14. Damages on CFRD model induced by G2-T2-0.59 g-SINE: (a) a picture; (b) a schematic drawing of the elevation view of the model after spin-down of the centrifuge.

I_a reaches 90.3 m/s, which is several times larger than that used in previous tests, making it possible to examine the failure mode under an extremely strong earthquake. The salient findings are summarized in the following.

The experimental results demonstrate two patterns of stress evolution in the face slab in terms of the overall trend during shaking. The first pattern is that compressive and tensile stress increments due to shaking are developed on the outer and inner faces, respectively. This occurs for the CFRDs which have not experienced a relatively strong earthquake. Such kind of stress evolution suggests that crushing of the face slab may emerge on the outer face, while tensile cracking may start from the inner face. The second pattern is that the inner face exhibits an overall tensile stress increment with time while the stresses on the outer face only fluctuate around zero with minor overall variation. This occurs when the CFRDs have experienced a relatively strong earthquake. Moreover, the stress evolution is related to the pattern of energy buildup during shaking and most of the variation occurs during the period with high rate of energy buildup. As for the spatial distribution of the stress increment along the face slab, there is larger stress increment near dam crest. In addition, the peak tensile stress increments due to shaking increase with increasing PGA.

For a CFRD subjected to an extremely strong earthquake, deep

sliding may occur and large volume of rock-fills near dam crest may move towards the downstream direction. In this study, the rock-fills originally located near dam crest with a height about 15% of the dam height have moved towards the downstream direction and then are loosely distributed on the original dam surface for an earthquake with a final Arias Intensity of 90.3 m/s. The damage evolution can be divided into three stages. Only slight surface sliding occurs and the dam deformation is limited in the first stage. Deep sliding occurs in the second stage and the associated rock-fill deformation contributes to most of the deformation induced by shaking. In this stage, the rock-fill particles move in a relatively large velocity, and the rock-fill near original dam crest seems move layer by layer towards the downstream direction. In the third stage, there is minor dam deformation. It is worth noting that the experiment is performed on a 0.21 m dam corresponding to a prototype dam having a height of 8.4 m, which is much smaller than the actual dam height ranging usually between 40 and 300 m. The slab thickness of the prototype 8.4m-high dam is 0.2 m, whereas the slab of a 120m-high dam is typically about 0.5 m, suggesting that the experiment uses a thicker slab compared to the slab of an actual CFRD. Hence, the conclusions of this study may not be applicable to actual CFRDs. However, the experimental results in this study can be indeed very useful for the verification of numerical models in CFRD analysis. In

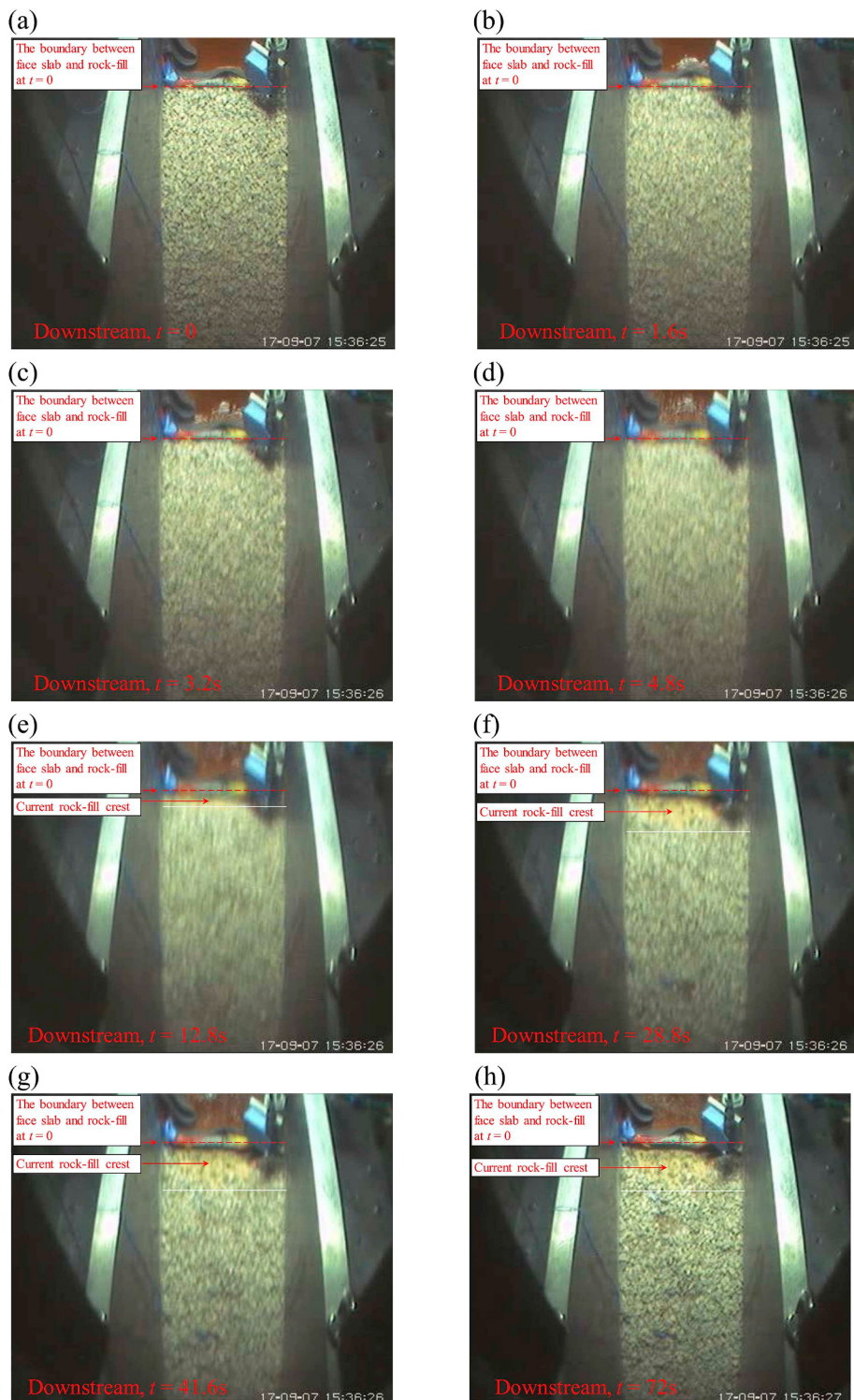


Fig. 15. Snapshots of the downstream rock-fill slope during G2-T2-0.59 g-SINE: (a) $t = 0$; (b) $t = 1.6\text{ s}$; (c) $t = 3.2\text{ s}$; (d) $t = 4.8\text{ s}$; (e) $t = 12.8\text{ s}$; (f) $t = 28.8\text{ s}$; (g) $t = 41.6\text{ s}$ and (h) $t = 72\text{ s}$.

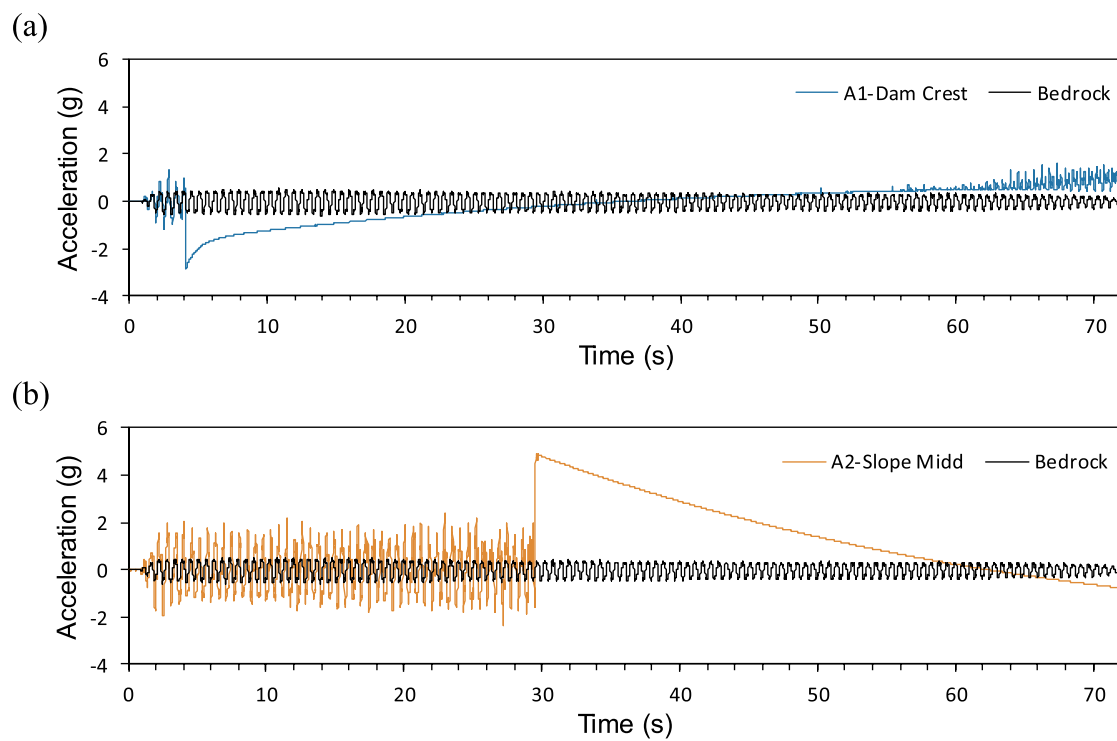


Fig. 16. Acceleration records at (a) dam crest and (b) at the middle of downstream slope during G2-T2-0.59 g-SINE.

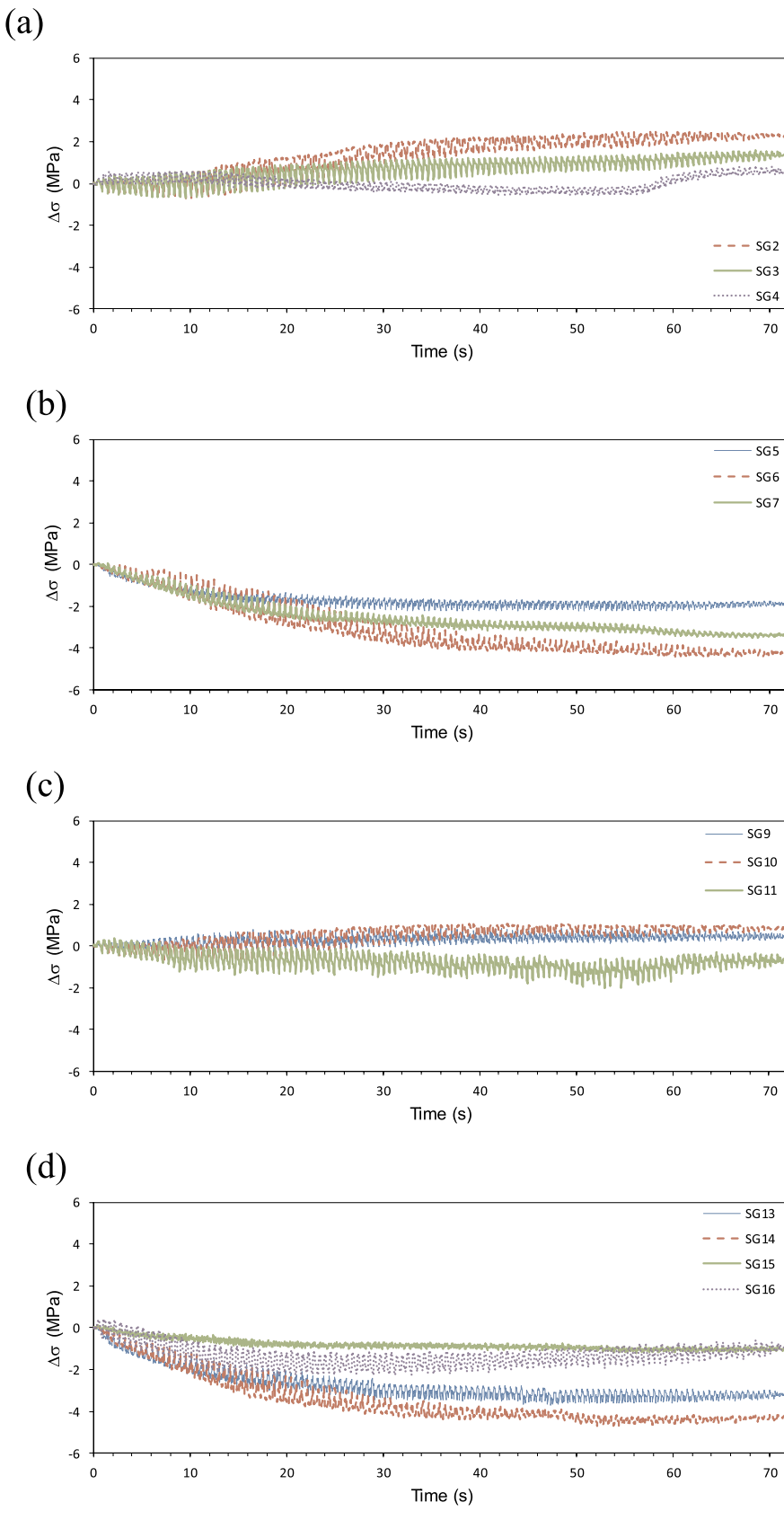


Fig. 17. Stress increments $\Delta\sigma$ due to shaking on the (a) outer and (b) inner faces of CS1 and on the (c) outer and (d) inner faces of CS2 during the dynamic test G2-T2-0.59 g-SINE.

addition, the seismic response of CFRDs is highly affected by the geometrical and material properties and the characteristics of the input motion, e.g., the frequency content and duration. Since only limited geometrical and material properties were utilized in this study, further experimental study is required to fully understand the seismic response of CFRDs and to draw universal conclusions.

Acknowledgements

This research was supported by National Key R&D Program of China (SQ2017YFSF060085), National Natural Science Foundation of China (51809290) and IWRH Research and Development Support Program (GE0145B122019 & GE0145B102017). The authors are grateful to our colleagues, Xu Z.P., Zhao J.M., Hou Y.J., Song X.H., Wu J.M. and Xing X., for their valuable suggestions and generous help in the preparation of the experiments. The authors are also grateful to reviewers for valuable comments.

References

- [1] Cooke JB, Sherard JL. Concrete-face rockfill dam: II. Design. *J Geotech Eng* 1987;113:1113–32.
- [2] Sherard JL, Cooke JB. Concrete-face rockfill dam: I. Assessment. *J Geotech Eng* 1987;113:1096–112.
- [3] Xing HF, Gong XN, Zhou XG, Fu HF. Construction of concrete-faced rockfill dams with weak rocks. *J Geotech Geoenviron Eng* 2006;132:778–85.
- [4] Seo MW, Ha IS, Kim YS, Olson SM. Behavior of concrete-faced rockfill dams during initial impoundment. *J Geotech Geoenviron Eng* 2009;135:1070–81.
- [5] Seiphoori A, Haeri SM, Karimi M. Three-dimensional nonlinear seismic analysis of concrete faced rockfill dams subjected to scattered P, SV, and SH waves considering the dam–foundation interaction effects. *Soil Dynam Earthq Eng* 2011;31:792–804.
- [6] Yang Z, Zhou J, Jiang G, Sun Y. Development of concrete faced rockfill dam in China. *Water Power* 2011;37:18–23. [in Chinese].
- [7] Xu Z. Key technical problems on the construction of super-high CFRD. *Water Power* 2010;36:51–9. [in Chinese].
- [8] Chen SS, Huo JP, Zhang WM. Analysis of effects of "5.12" Wenchuan earthquake on Zipingpu concrete face rock-fill dam. *Chin J Geotech EJ Geotech Eng* 2008;30:795–801. [in Chinese].
- [9] Guan ZC. Investigation of the 5.12 Wenchuan earthquake damages to the Zipingpu water control project and an assessment of its safety state. *Sci China E* 2009;52:820–34.
- [10] Chen SS, Han HQ. Impact of the '5.12'Wenchuan earthquake on Zipingpu concrete face rock-fill dam and its analysis. *Geomechanics Geoeng: Int J* 2009;4:299–306.
- [11] Han G, Kong X, Li J. Dynamic experiments and numerical simulations of model concrete-face rockfill dams. *Proceedings of ninth world conference on earthquake engineering*. 1988. p. 331–6. Tokyo-Kyoto, Japan, vol. I.
- [12] Liu X, Wang Z, Zhao J. Advancement of technology on shaking table model test and dynamic analysis of CFRD. *J Hydraul Eng* 2002;29–35. [in Chinese].
- [13] Zhou G, Liu X, Zhao J, Liu Q, Yang Y, Yang Z. The shaking table model test study on acceleration seismic response of Zipingpu CFRD. *China Civ Eng J* 2012;45:20–4. [in Chinese].
- [14] Uddin N, Gazetas G. Dynamic response of concrete-faced rockfill dams to strong seismic excitation. *J Geotech Eng* 1995;121:185–97.
- [15] Bayraktar A, Hacioglu K, Muvafov M. Asynchronous seismic analysis of concrete-faced rockfill dams including dam–reservoir interaction. *Can J Civ Eng* 2005;32:940–7.
- [16] Kong X, Zhou Y, Zou D, Xu B, Yu L. Numerical analysis of dislocations of the face slabs of the Zipingpu concrete faced rockfill dam during the Wenchuan earthquake. *Earthq Eng Eng Vib* 2011;10:581–9.
- [17] Zou D, Zhou Y, Ling HI, Kong X, Xu B. Dislocation of face-slabs of Zipingpu concrete face rockfill dam during Wenchuan earthquake. *J Earthq. Tsunami* 2012;6:1250007.
- [18] Dakoulas P. Nonlinear seismic response of tall concrete-faced rockfill dams in narrow canyons. *Soil Dynam Earthq Eng* 2012;34:11–24.
- [19] Zou D, Xu B, Kong X, Liu H, Zhou Y. Numerical simulation of the seismic response of the Zipingpu concrete face rockfill dam during the Wenchuan earthquake based on a generalized plasticity model. *Comput Geotech* 2013;49:111–22.
- [20] Cheng S, Zhang J. Dynamic centrifuge model test on concrete-faced rockfill dam. *J Earthq Eng Eng Vib* 2011;31:98–102. [in Chinese].
- [21] Wang NX, Zhang WM. Centrifuge model test for seismic response of concrete face rock fill dam. *Hydro-Sci Eng* 2003;1:18–22. [in Chinese].
- [22] Cheng S, Zhang J. Centrifuge modeling test of dynamic response and deformation law of concrete-faced rockfill dam. *Eng Mech* 2012;29:2982–5. [in Chinese].
- [23] Kim MK, Lee SH, Yun WC, Kim DS. Seismic behaviors of earth-core and concrete-faced rock-fill dams by dynamic centrifuge tests. *Soil Dynam Earthq Eng* 2011;31:1579–93.
- [24] Hou YJ, Zhang XD, Xu ZP, et al. Performance of horizontal and vertical 2D shaker in IWHR centrifuge. *Proceedings of the 8th international conference on physical modelling in geotechnics (ICPMG2014)*. 2014. p. 207–13. Perth, Australia, 14–17 January 2014.
- [25] Park DS, Kim NR. Safety evaluation of cored rockfill dams under high seismicity using dynamic centrifuge modeling. *Soil Dynam Earthq Eng* 2017;97:345–63.
- [26] Seed HB, Wong RT, Idriss IM, Tokimatsu K. Moduli and damping factors for dynamic analyses of cohesionless soils. *J Geotech Eng* 1986;112:1016–32.
- [27] NB 35047 – 2015. Code for seismic design of hydraulic structures of hydropower project. 2015. [in Chinese].
- [28] Dashti S, Bray JD, Pestana JM, Riemer M, Dan W. Mechanisms of seismically induced settlement of buildings with shallow foundations on liquefiable soil. *J Geotech Geoenviron Eng* 2010;137:151–64.